3rd Conference on Sustainability in Civil Engineering (CSCE'21)
Department of Civil Engineering
Capital University of Science and Technology, Islamabad Pakistan

STRUCTURAL PERFORMANCE OF GFRP-REINFORCED BCJ THROUGH FINITE ELEMENT ANALYSIS

[a] Anees ur Rehman*, [b] Qaiser uz Zaman Khan, [c] Ali Raza

a: Department of Civil Engineering, University of Engineering and Technology Taxila, 47080, Pakistan, engr.anees6384@gmail.com
b: Department of Civil Engineering, University of Engineering and Technology Taxila, 47080, Pakistan, dr.qaiser@uettaxila.edu.pk
c: Department of Civil Engineering, University of Engineering and Technology Taxila, 47080, Pakistan
* Corresponding author: Email ID: ali.raza@uettaxila.edu.pk

Abstract- Glass-fiber reinforced polymer (GFRP) rebars are being employed as a good substitute to steel in reinforced concrete (RC) structural elements due to their superior performance. The main objective of the present study is to evaluate the structural behavior of beam-column joints (BCJ) reinforced with GFRP rebars using non-linear finite element analysis (NLFEA) under the seismic loading. In the present study, three-dimensional NLFEA of BCJ reinforced with steel and GFRP rebars was conducted using a finite element (FE) code ABAQUS. The FE model was verified against the experimental load-deflection curves of BCJ. A sensitivity analysis of the proposed FE model was carried out to investigate the effect of different parameters, including mesh size, dilation angle (ψ), stress ratio, viscosity parameter (VP), eccentricity, and shape factor of concrete material on the load-deflection response of BCJ. The FE modeling using ABAQUS software predicted the experimental load-deflection curve of BCJ with sufficient accuracy. The results concluded that the currently proposed FE model can accurately pretend the load-deflection performance of BCJ.

Keywords- GFRP; finite element modeling; concrete damaged plasticity; BCJ; failure modes; parametric study

1 Introduction

The GFRP rebars are now utilized everywhere in the world as a viable substitution to steel in current substantial constructions particularly in such designs that may bear severe environmental conditions [1]. The majority of the past research shows that fiber-reinforced polymers (FRPs) are a functioning swap for steel while giving a few benefits like corrosion resistance, including high strength, simplicity of taking care of, high tensile strength, low self-weight, and low maintenance necessity [2-4]. In any case, brittle performance is a significant shortcoming of FRP rebars because of which they show straight elastic conduct up to rupture, which seriously influences the ductility of concrete. Considering the shortfall of ductility, FRPs portray low value of modulus when compared with ordinary steel. This performance of FRP achieves excessive deflections and large cracks that affect its functionality [5]. To look at the thermal stability of glass fiber reinforced polymer (GFRP) rebars, it was seen that mechanical characteristics like shear, flexural, and ductile improvement with the decline in temperature [6]. The external surface conditions like ribbed GFRP rebars and string-wrapped were generally influencing the bond strength and pullout behavior of GFRP rebars [7].

Various experimental studies have been carried out on the beam-column joints (BCJ) reinforced with either steel rebars or GFRP rebars under different seismic loading conditions [8-23]. These studies concluded that the structural performance of BCJ can be significantly improved by using advanced FRP composites. A detailed investigation of the role of GFRP reinforcement in the perpendicular beam of BCJ concluded that the capacity of BCJ can be enhanced when GFRP reinforcing rebars are added to the perpendicular beams [24, 25]. The GFRP reinforced columns show a smaller axial load and bending moment capacity as compared to conventional steel-reinforced columns. On the other hand, the ductility of

the GFRP reinforced columns was very close to the ductility of the steel-reinforced columns [26]. Benmokrane et al. [27] experimented and concluded that the flexural conduct of beams utilizing various kinds of GFRP rebars in a 3.3 m long rebar and contrasted exploratory outcomes with the conservative steel rebars. The outcomes demonstrate that GFRP rebars are a favorable choice for steel. GFRP-RC beams display larger stiffening strain-hardening and bigger crack widths when contrasted with steel having lower stiffness of GFRP rebars [28]. A non-linear finite element analysis (NLFEA) was carried out to consider the buckling in I-beams and reasoned that because of the end bending constraints and amendment in loading capacity, the FRP rebar portray larger effects the buckling process when contrasted with steel [29, 30]. The finite element (FE) crack samples of geopolymer concrete flexural members showed a nearby concurrence with the tests, however, introduced a few deviations in the deflection results [31]. The mathematical outcomes got from NLFEA for the shear limit and crack samples of outside and inside BCJ gave a decent understanding of testing results [32]. Elflah et al. proposed a NLFEA model on hardened steel BCJ which precisely anticipated stiffness, maximum resistance, moment rotation performance, and the failure patterns [33]. A mathematical examination of non-ductile external joints has been carried out to investigate the shear breaking. Mathematical outcomes demonstrate that joint perspective proportion and rebar longitudinal support proportion were the significant boundaries that impact the joint shear behavior [34]. The performance of a BCJ was researched by utilizing ABAQUS programming. An identical T-stub strategy was utilized to demonstrate every one of the components of the tension areas of the BCJ concluding that the tension joint presented an increment in deflections [35].

The literature review depicts that the NLFEA modeling of steel and GFRP built up BCJ has not been performed in the previous studies on BCJ and, therefore, there is a need to investigate the performance of GFRP-RC BCJ to positively validate their applications in the construction industry which is the novelty of the present work. The main goal of the current examination is to propose a three-dimensional NLFEA model utilizing ABAQUS that precisely predicts the underlying performance of GFRP built-up BCJ. The subsequent goal is to execute an extensive parametric examination utilizing the proposed constitutive NLFEA model to analyze the impact of different geometric and material boundaries of BCJ. Finally, the cracking patterns and failure modes of concrete in BCJ were reviewed. This examination will be useful for designers to investigate and design the GFRP reinforced concrete BCJ utilizing the suggested NLFEA model. Furthermore, the serviceability of structures will be improved using FRP in structural elements.

2 Finite Element Analysis

Joints elements were modeled using commercial software ABAQUS 6.12 [36], a general NLFEA program is employed to verify the influence of GFRP rebars on BCJ. In the preprocessing stage, material properties, element types, geometry, and boundary conditions, and nonlinear analysis solutions are defined. There are different models in ABAQUS which are employed to define the structural performance of concrete as a quasi-brittle material, i.e., brittle and smeared cracking models. In the damage plasticity model, yield criteria, hardening rule, and flow rule are essential integrals of the model [34]. By using the experimental results of Mohammad et al. [1], this study investigated the numerical models of the BCJ by calibrating the key factors like reinforcement types and ratios. The structural dimensions of the studied BCJ, as shown in Figure 1, are summarized in having a horizontal beam with a cross-section of 350 mm ×450 mm and a vertical column with a 350 mm × 500 mm cross-section. The height of the column is 3650 mm, and the length of the beam is 2350 mm.

In the present study, the testing samples SS, GS, and GS3 were labelled as MSS, MGS, and MGS3, correspondingly [1]. The details of the longitudinal and shear reinforcement of all specimens are shown in Table 1. All test samples were made with a maximum aggregate size of 20 mm using normal weight ready mix concrete. The obtained 28-days compressive strength of concrete specimens was determined based on a standard cylinder test was 32 MPa. The properties of reinforcing rebars are shown in Table 2. Figure 2 shows the simulated FE models of BCJ.

Table 1. Reinforcement details of specimens

Specimens	Beam		Column	
	Rebars	Stirrups	Rebars	Stirrups
Specimen (MSS)	5#M20 Steel	2 legs steel hoop #10M@100 mm	8#M15 Steel	2 legs steel hoop #10M@90 mm +1 transversal crosstie #10M@90 mm
Specimen (MGS1)	5#16 GFRP	3 branches #13GFRP@100 mm	8#16 GFRP	3 branches #13GFRP@90 mm +1 transversal branch #10GFRP@90 mm
Specimen (MGS3)	8#19 GFRP	3 branches #13GFRP@100 mm	12#19 GFRP	3 branches #13GFRP@90 mm +1 transversal branch #10GFRP@90 mm

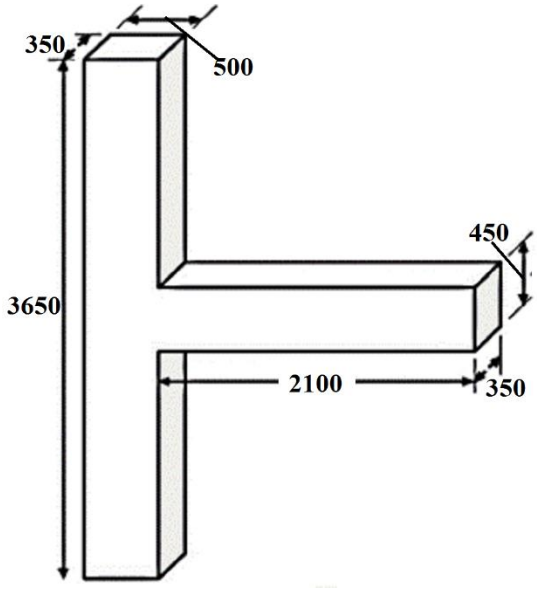

Figure 1. Overall dimensions of the specimen (all values are in mm)

Table 2. Properties of steel and GFRP Rebars

Rebar Size	Young's Modulus (GPa)	Tensile strength (MPa)
Steel #20M	200	f_y=400 (460)^a
Steel #15M	200	f_y=400 (460)^a
Steel #10M	200	f_y=400^a
GFRP #19	47.6	728
GFRP #13	46	590^b
GFRP #10	45	642^b

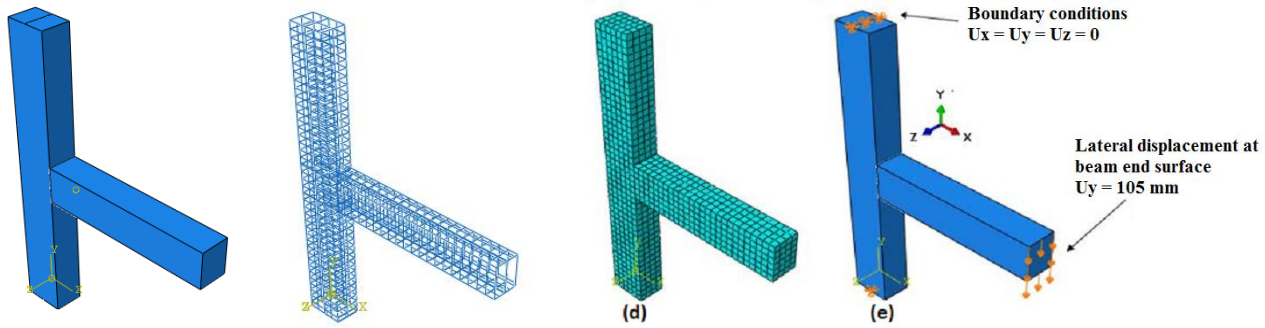

Figure 2. Simulated FE models

2.1 Concrete damage plasticity (CDP) model

The numerical simulation of concrete is a challenging task because of the complex behavior of concrete under loading. In this work, using the concept of isotropic damaged elasticity combine with compressive plasticity and isotropic tensile the inelastic behavior of concrete was presented by a CDP model. The strain hardening under compressive loading can be determined by using the CDP model based on the strain rate. The elastic behavior of confined concrete is up to 50% of peak confined loading strength. Therefore, to consider the confinement improvement effect due to GFRP ties, the models suggested by Afifi et al. [37] for the compressive stress and compressive strain of confined concrete were employed in this research as portrayed by Eq. (1) and Eq. (2).

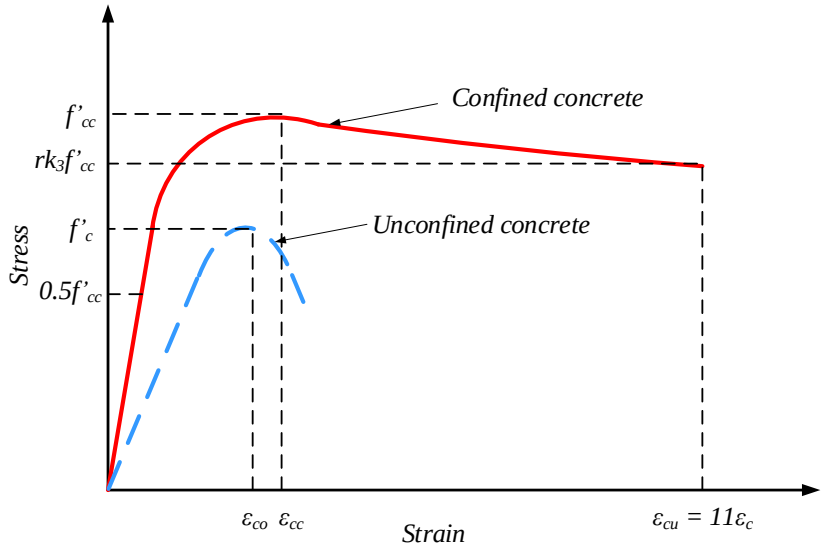

Figure 3. Stress-strain performance of confined and unconfined concrete

$$\frac{f'_{cc}}{f'_{co}} = 1.0 + 4.547\left(\frac{f_{le}}{f'_{co}}\right)^{0.723} \quad (1)$$

$$\frac{\varepsilon'_{cc}}{\varepsilon'_{co}} = 1.0 + \left(\frac{0.024}{\varepsilon'_{co}}\right)\left(\frac{f_{le}}{f'_{co}}\right)^{0.907} \quad (2)$$

where f_{le} reports the effective confinement loading strength provided by the GFRP ties which can be measured from Eq. (3) [38].

$$f_{le} = \frac{2E_f \varepsilon_{h,rup} t}{D} \quad (3)$$

where E_f describes the elastic modulus of lateral ties, $\varepsilon_{h,rup}$ describes the hoop rupture strains of lateral GFRP ties and 't' defines the thickness of lateral GFRP ties. According to the concept of elastoplasticity theory, the total strain of concrete (ε) can be divided into two parts: the elastic strain (ε^{el}) and the plastic strain (ε^{pl}) of concrete as portrayed by Eq. (4).

$$\varepsilon = \varepsilon^{el} + \varepsilon^{pl} \quad (4)$$

The uniaxial compression damage parameter (d_c) and the uniaxial tension damage parameter (d_t) are employed for the simulation of damage of concrete in the CDP model. By assuming Figure 4, the compressive (σ_c) and tensile (σ_c) strengths of concrete can be calculated as:

$$\sigma_c = (1 - d_c)E_o\left(\varepsilon_c - \varepsilon_c^{pl}\right) \quad (5)$$

$$\sigma_t = (1 - d_t)E_o\left(\varepsilon_t - \varepsilon_t^{pl}\right) \quad (6)$$

where E_o is Young's modulus of concrete, ε_c is the compression strain of concrete, and ε_c^{pl} is the plastic portion of the compression strain of concrete and ε_t^{pl} is the plastic portion of the tension strain of concrete. The factor d_c and d_t are defined by Eq. (7) and Eq. (8), correspondingly [39].

$$d_c = \frac{1}{e^{-1/m_c - 1}}\left(e^{-\varepsilon_{c,norm}^{in}/m_c} - 1\right) \quad (7)$$

$$d_t = \frac{1}{e^{-1/m_t - 1}}\left(e^{-\varepsilon_{t,norm}^{ck}/m_t} - 1\right) \quad (8)$$

where m_c is the compressive collapse progression speed governing parameter with a value of 0.1 and m_t is the tensile collapse evolution speed governing parameter with a value of 0.05 [40]. The parameter $\varepsilon_{c,norm}^{in}$ is the standardized compressive plastic strain that can be interpreted by the ratio of inelastic compressive strain having a value of 0.033 $\varepsilon_{c,norm}^{in}$ is the standardized tensile plastic strain of concrete having a value of 0.0033 [40].

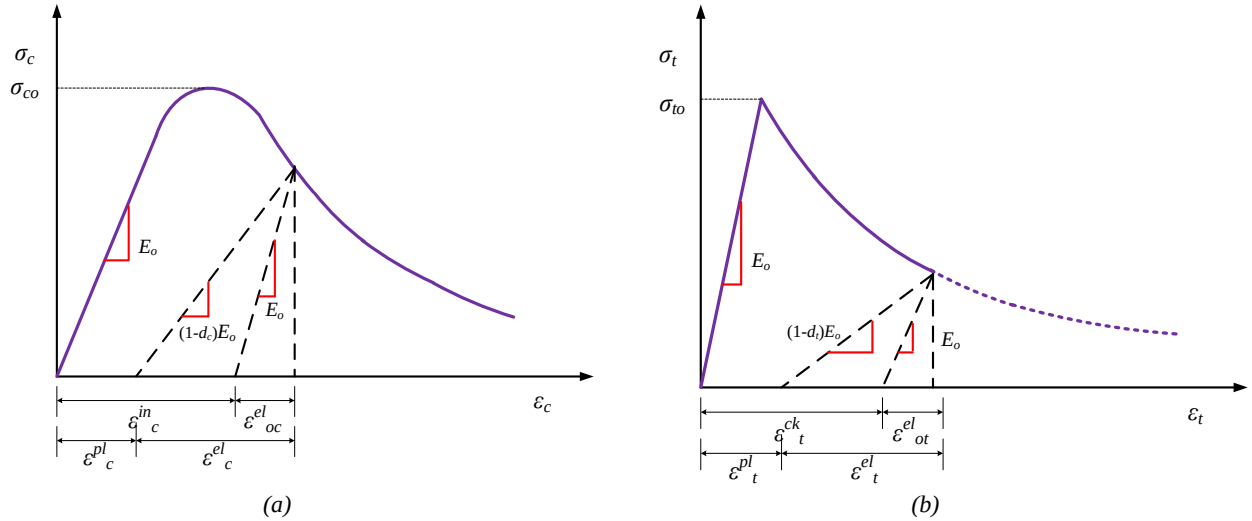

Figure 4. (a) Compressive stress-strain behavior of concrete (b) Tensile stress-strain behavior of concrete

The compressive and tensile loading strength, the Poisson's ratio v and the Young's modulus E_0 are some concrete mechanical behavior parameters. The value of Poisson's ratio $v = 0.2$ is assumed as constant for the CDP model in this

work. The corrected values were taken for dilation angle (ψ) and viscosity parameter (VP) and shape factor K_c=0.667, eccentricity ε =0.1, the stress ratio σ_{b0}/σ_{c0}=1.16 are the default values employed for the CDP model in ABAQUS [41]. The non-linearity of the concrete is produced from three major causes: the ductility of the steel reinforcement, the nonlinearity of the concrete under compressive loading, and the behavior of the concrete in the tension zones [41]. The values of ultimate stress and ultimate stain and yielding are taken from experimental results [1]. The nonlinear response of reinforcing rebars was assumed to be linear elastic-perfectly plastic. The value of Poisson's ratio v was taken as 0.3.

2.2 Calibration of a model on material parameters

The calibration of the FE model is done according to the experimental test results. For the justification of the numerical model, different materials and geometric parameters were investigated to obtain a result that is closer to the experimental results. Here, specimen MSS is selected as a control sample and VP, element type, ψ, eccentricity, stress ratio, shape factor, and mesh size are the varying parameters. After calibration, the model is then employed to perform FEM analysis on other specimens. Element types C3D8R and T3D2 were employed for concrete and reinforcement, correspondingly. Concrete is usually considered a brittle material and due to inelastic strains undergo considerable volume change which is called dilatancy. By assigning the value of ψ, dilatancy can be modeled in the CPD model, according to the researcher's ψ is ranges between 31∘ to 42∘ [42-45]. A sensitive FE examination is executed to consider the impact of ψ on load-deflection performance. Figure 5 reports that the ψ somewhat influences the load-deflection curve. With the increment in ψ, the maximum load improves, and it was seen that the ψ of 35◦ reported a negligible effect on the load-deflection behavior of the test curves. In this way, a ψ of 35∘ was preferred for all remaining investigations with VPs and meshing sizes of 0.0075 and 80 mm, separately. Eventually, it can undoubtedly be reasoned that larger amounts depict ductile performance and small values of the ψ depict lower performance [32]. The eccentricity (ε) was validated to examine a maximum load-deflection of the BCJ as shown in Figure 5. Various values of (0.1, 0.2, 0.3 and 0.4) were chosen to examine the load-deflection curves. The outcomes show that the impact of ε on the BCJ samples is minor.

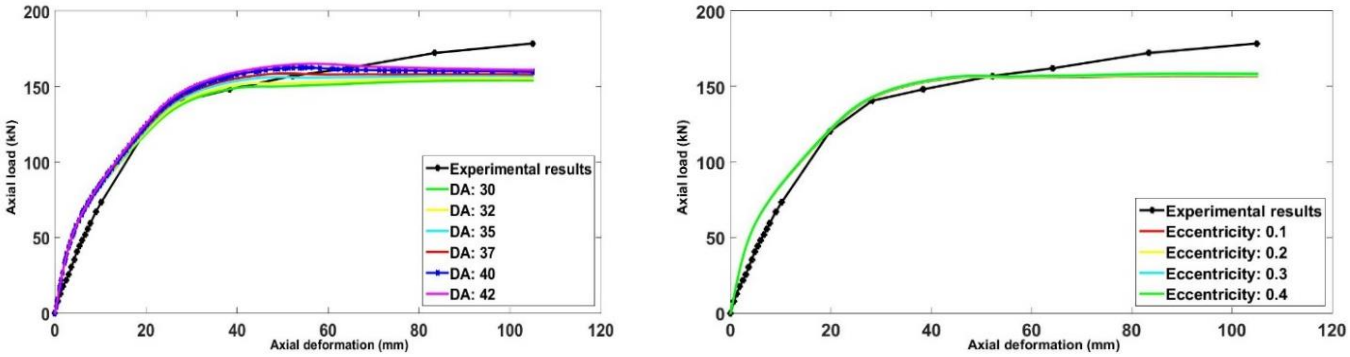

(a) (b)

Figure 5. Calibration work (a) effect of ψ on the load-deflection performance (b) effect of eccentricity on load- deflection performance

The validation process for the stress ratio was also carried out to examine the consequence of different stress ratios σ_{b0}/σ_{c0} value. The predictions of the NLFEA model show that change of values is not showing any protruding change, so 1.16 was selected which was also the default value [46]. To explore the performance of parameter Kc, some validation works have been made. To simulate the yielding surface and shape, the Kc parameter is very important. By default, it is considered to carry a value of 0.667 although its range is between 0.5 to 1 [32]. In the current investigation, four various quantities of shape factor were selected as 0.667, 0.750, 0.822, and 1.0. Therefore, the most precise predictions can be employed as the default value of 0.667. To inspect the effect of mesh size, its values of 140 mm, 120 mm, 100 mm, 80 mm, 60 mm, and 40 mm were employed to examine the influence of various mesh sizes on the NLFEA model. Figure 6 shows that mesh size 80 mm represents a more precise outcome compared with the test load-deflection curve.

To examine the impact, various values of VP (VP) 0.0015, 0.0035, 0.0055, 0.0075, 0.0095, and 0.015 were utilized in the NLFEA model. By utilizing the VP of 0 (which is the default ABAQUS esteem), the modeling will end. The value of the VP relies on the time increase step, the scientist proposes that to increase the arrangement 15% of the time increase step value is to be selected [46]. Various amounts of the VP greatly influence the load-deflection behavior as represented in Figure 7. The best fit to experimental results is obtained unison 80 mm and 35° for mesh size and dilation of concrete, correspondingly.

3 Discussion of Results

3.1 Load-deflection response

After validating the control model for various parameters, the calibrated control model MSS was employed to remaining BCJ members to examine the performance of the load-deflection behavior as represented in Figure 8(a & b). Figure 8 shows that steel rebars portrayed a close correlation with the test outcomes as associated to GFRP rebars. But some differences are observed in the load-deflection curve at ultimate load failure as shown in Figure 8(a) because, in FEM, the concrete is considered as a homogenous type of material, but the experimental concrete is not homogenous. The specimen MGS and MGS 3 as shown in Figures 8 (a) and (c) show more stiffness than the experimental curve. This may be due to the difference in the boundary condition of actual and tested specimens and the assumption of perfect bond during FEA and the accuracy of the testing instruments. The calibration work also reported a good response for the complete load-deflection curves of the BCJ specimens.

Although the proposed numerical model reported a good prediction behavior in the elastic behavior, it portrayed some differences in the post-peak behavior of the load-deflection curves. The minor deviations between the experimental and NLFEA results can be credited to the following reasons: (1) deviations in materials properties provided by the manufacturers (2) assumptions made during NLFEA simulations for the materials definitions (3) considering the linear elastic behavior of GFRP rebars (4) assuming perfect bond between the concrete and reinforcement, and (5) assumptions of boundary conditions made in the NLFEA simulations [47-52].

3.2 Cracking patterns

In the MSS specimen cracks produced in the plastic hinges zone prolonged from the face of the column to the death of the beam and no cracks seemed in the column or joint area as represented in Figure 9(a). Figure 9(b) shows that failure occurs gradually starting with spalling of concrete. In specimen MGS the GFRP rebars portrayed rupture at the deflection of 136.5 mm of the beam. The GFRP stirrups presented the failure after the peak loading capacity when the concrete core was activated after securing the ultimate strength of concrete. In specimen MGS 3 at the joint area a larger diagonal failure look, the crack becomes wider and ongoing to proceed toward the far edge of the column as shown in Figure 9(c).

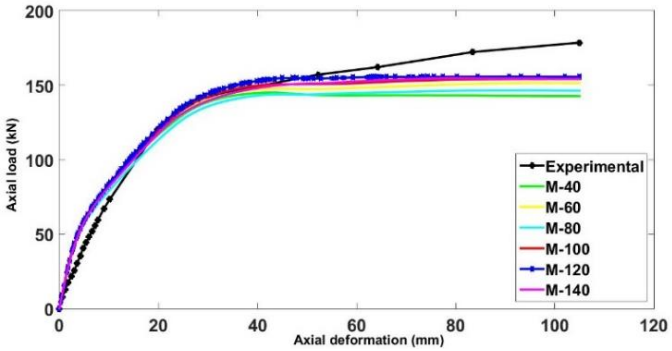

Figure 6. Lateral load deflection for various mesh values.

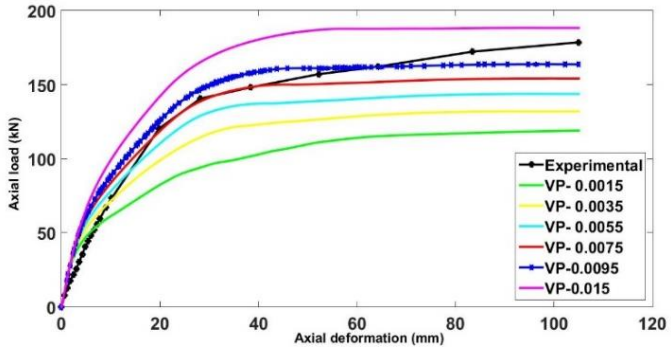

Figure 7. Load-deflection response for various values of VP.

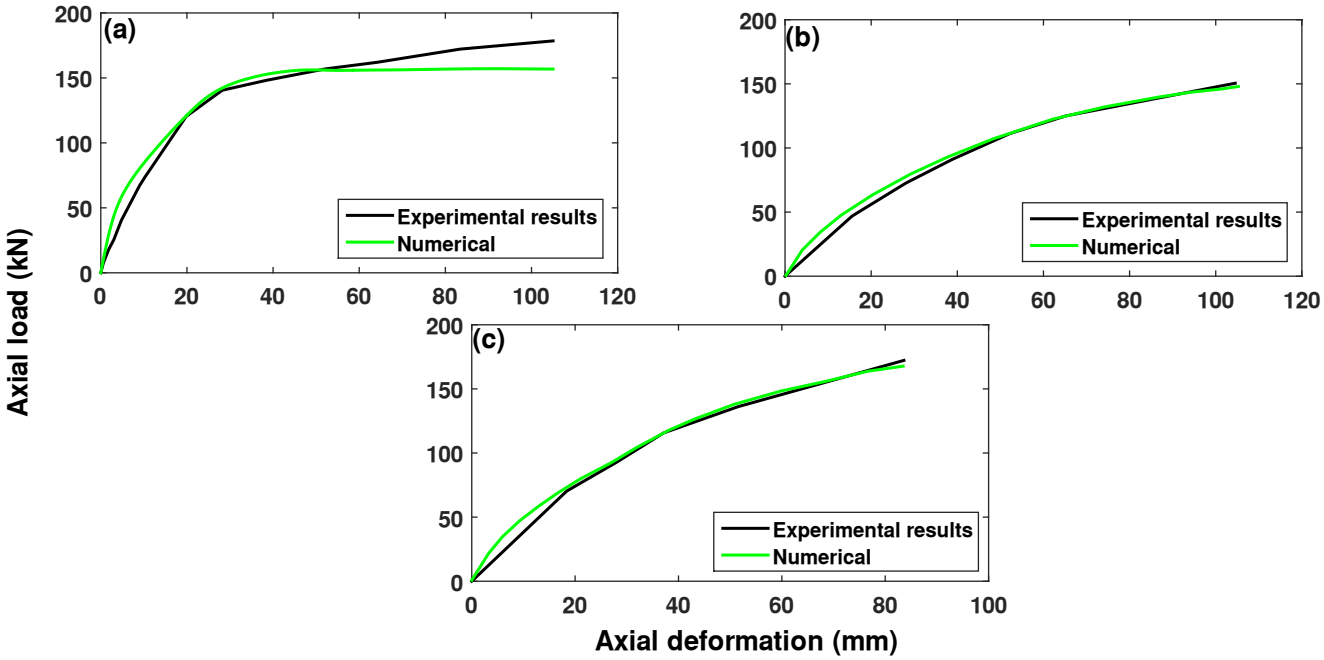

Figure 8. NLFEA and test load-deflection behavior of (a) MSS (b) MGS (c) MGS3.

By employing the CDP, the cracks performance of concrete will happen because of the positive ultimate principal plastic straining. The track of the cracks process is observed via ultimate principal plastic straining due to the reason that direction of the cracking process is considered as normal to the ultimate principal plastic straining [41, 42, 52, 53]. Crack behavior and failure modes of steel and GFRP BCJ are represented in Figure 9 which was secured from NLFEA modeling in ABAQUS. The crack patterns obtained from the proposed NLFEA model depict a good correlation with test cracks in the joint region. The failure of the specimens was mostly observed at the connection of columns to beam due to the rupture of GFRP bars in GFRP reinforced BCJ and the yeilding/buckling of steel bars in the steel rebars renforced BCJ soecimens. The brottle behavior of GFRP rebars allowed them to rupture after reaching to their ultimate tensile strength. Similar observations were depicted by the proposed NLFEA model in the present study.

4 Practical Implementation of Present Work

The beam-column joint is very important structural part that bears the stress concentrations during any uncertainty in the loading due to the earthquake or any other uncertain conditions. This study proposes a novel nonlinear finite element model that can accurately predict the structural behavior (including load-deflection response and failure behavior) of beam-columns joints reinforced with advanced fiber reinforced polymers. This study will be helpful for the structural engineers in understanding the load-deflection behavior, complex damaging behavior, and failure behavior under the cyclic loading without performing the costly experimentation. Moreover, the good outcomes of the present investigation will be helpful for the practitioners in Pakistan in implementing the corrosion-resistant and lightweight GFRP material in structural elements.

5 Conclusions

The present study aims to evaluate the structural behavior of beam-column joints (BCJ) reinforced with GFRP rebars using non-linear finite element analysis (NLFEA) under the seismic loading. The following conclusions can be drawn from the present work:

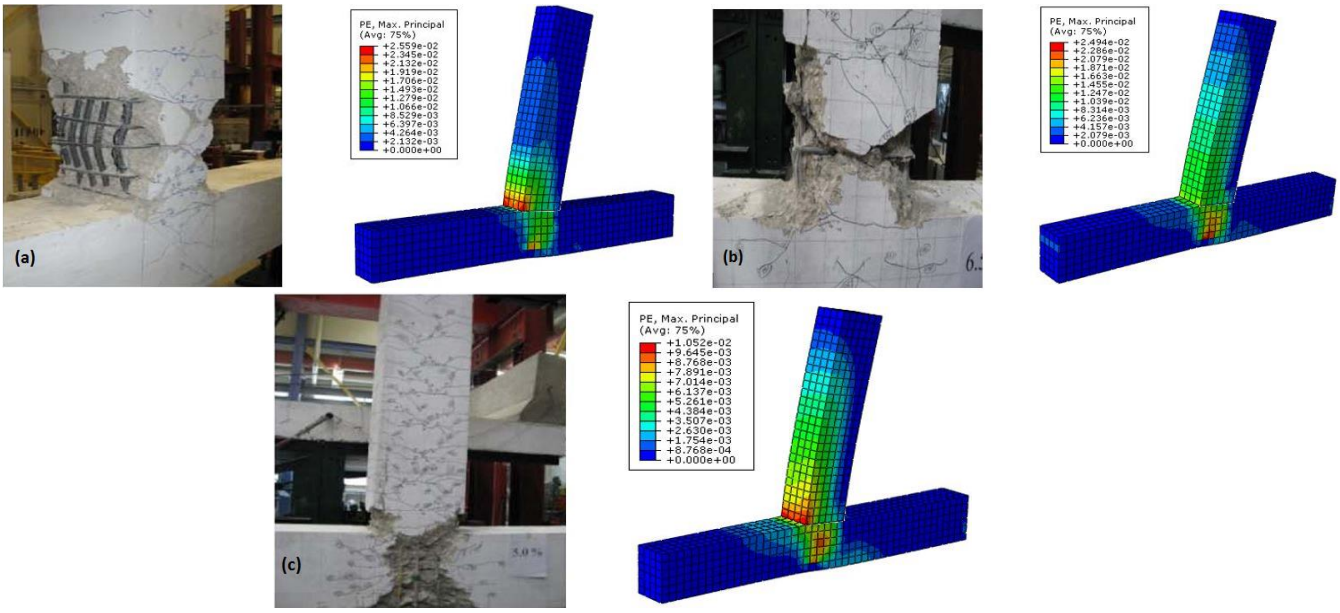

Figure 9. Crack patterns of (a) MSS (b) MGS (c) MGS3

- The results indicated that the FEA utilizing ABAQUS computer program is capable to anticipate the load-deflection curves in BCJ reinforced with steel and GFRP rebars having acceptable accuracy of 87.85%.
- Various material parameters such as mesh, dilation angle ψ, shape factor, and viscosity parameter VP have been considered for the calibration of the behavior of concrete modeling which depicted that the calibration work is very important for the NLFEA simulations to secure the better results compared with the experimentation work. Among the studied parameters, the VP reported a critical influence on concrete modeling utilizing the CPD model. The variation of VPs provides more exact results for the complete load-deflection behavior of BCJ. Mesh size ranging between 40 mm to 140 mm has signifying effect on the load-deflection curves response by affecting the computational time of the computer, the greater value of the mesh size decreased the computational time.
- The varying values of VPs from 0.0015 to 0.015 can significantly affect the computational time and load-deflection curve behavior, a smaller value of the VP increases the computational time of the computer. The change in dilation angle, meshing, and types of steel and concrete elements portrayed the least impact on the load-deflection behavior of BCJ. Finally, it can be said that the proposed numerical model can accurately predict the behavior of GFRP-reinforced BCJ and can be employed for the practical applications.

Acknowledgment

The authors are thankful to the UET Taxila for the provision of the facility of CAD Lab for the finite element simulations. The authors acknowledge Dr. Afaq Ahmad for his kind help and support in performing finite element simulations. The careful review and constructive suggestions by the anonymous reviewers are gratefully acknowledged

References

[1] M, Mady, A. El-Ragaby, and E. El-Salakawy, "Seismic behavior of beam-column joints reinforced with GFRP bars and stirrups." *Journal of Composites for Construction*, 15(6): p. 875-886, 2011.

[2] C.E. Bakis, et al., "Fiber-reinforced polymer composites for construction—State-of-the-art review. " *Journal of composites for construction*, 6(2): p. 73-87, 2002.

[3] J. Correia, et al., "Durability of pultruded glass-fiber-reinforced polyester profiles for structural applications." *Mechanics of Composite Materials*, 42(4): p. 325-338, 2006.

[4] Y. Bai, et al., "Experimental investigations on temperature-dependent thermo-physical and mechanical properties of pultruded GFRP composites." *Thermochimica Acta*, 469(1-2): p. 28-35, 2008.

[5] A. El Refai, F. Abed, and A. Al-Rahmani, "Structural performance and serviceability of concrete beams reinforced with hybrid (GFRP and steel) bars." *Construction and Building Materials*, 96: p. 518-529, 2015.

[6] M. Robert, and B. Benmokrane, "Behavior of GFRP reinforcing bars subjected to extreme temperatures." *Journal of Composites for Construction*, 14(4): p. 353-360, 2009.

[7] M. Harajli, and M. Abouniaj, "Bond performance of GFRP bars in tension: Experimental evaluation and assessment of ACI 440 guidelines." *Journal of Composites for Construction*, 14(6): p. 659-668, 2010.

[8] B. Roy, and A.I. Laskar. "Cyclic performance of beam-column subassemblies with construction joint in column retrofitted with GFRP." in *Structures*. Elsevier, 2018.

[9] S.K. Ghomi, and E. El-Salakawy, "Effect of joint shear stress on seismic behaviour of interior GFRP-RC beam-column joints." *Engineering Structures*, 191: p. 583-597, 2019.

[10] H. Huang, et al., "Seismic behavior of a replaceable artificial controllable plastic hinge for precast concrete beam-column joint." *Engineering Structures*, 245: p. 112848, 2021.

[11] J.H. Kim, et al. "Experimental study on lateral behavior of post-tensioned precast beam-column joints." *in Structures*. Elsevier, 2021.

[12] K. Sakthimurugan, and K. Baskar, "Experimental investigation on rcc external beam-column joints retrofitted with basalt textile fabric under static loading." *Composite Structures*, 268: p. 114001, 2021.

[13] H. Wang, et al., "Cyclic behavior and hysteresis model of beam-column joint under salt spray corrosion environment." *Journal of Constructional Steel Research*, 183: p. 106737, 2021.

[14] J.G. Ruiz-Pinilla, et al., "RC columns strengthened by steel caging: Cyclic loading tests on beam-column joints with non-ductile details." *Construction and Building Materials*, 301: p. 124105, 2021.

[15] P. Sachdeva, A.D. Roy, and N. Kwatra. "Behaviour of steel fibers reinforced exterior beam-column joint using headed bars under reverse cyclic loading." in *Structures*. Elsevier, 2021.

[16] A.B. Ugale, and S.N. Khante. Hysteretic performance of reinforced concrete external beam-column joint subassemblies using non-conventional diagonal bars. in *Structures*. Elsevier, 2021.

[17] A.S. Borujerdi, D. Mostofinejad, and H.-J. Hwang, "Cyclic loading test for shear-deficient reinforced concrete exterior beam-column joints with high-strength bars." *Engineering Structures*, 237: p. 112140, 2021.

[18] S. Chen, K. Chen, and K.H. Tan, "Effect of profiled decking on composite beam-column joints with end-plate bolted connections under column-removal scenario." *Journal of Constructional Steel Research*, 182: p. 106668, 2021.

[19] Z. Chen, et al., "Seismic study on an innovative fully-bolted beam-column joint in prefabricated modular steel buildings." *Engineering Structures*, 234: p. 111875, 2021.

[20] R.Z. Al-Rousan, and A. Alkhawaldeh, "Behavior of Heated Damaged Reinforced Concrete Beam-Column Joints Strengthened with FRP." *Case Studies in Construction Materials*, p. e00584, 2021.

[21] X. Gao, and C. Lin, "Prediction model of the failure mode of beam-column joints using machine learning methods." *Engineering Failure Analysis*, 120: p. 105072, 2021.

[22] C.-K. Chiu, D.P. Lays, and W.A. Krasna, "Anchorage strength development of headed bars in HSRC external beam-column joints considering side-face blowout failure under monotonic loading." *Engineering Structures*, 239: p. 112218, 2021.

[23] S. Majumder, and S. Saha. "Quasi-static cyclic performance of RC exterior beam-column joint assemblages strengthened with geosynthetic materials." in *Structures*. Elsevier, 2021.

[24] L. Eddy, et al., "Analytical investigation of the role of reinforcement in perpendicular beams of beam-column knee joints by 3D meso-scale model." *Engineering Structures*, 210: p. 110347, 2020.

[25] J. Bian, et al. "Cyclic loading tests of thin-walled square steel tube beam-column joint with different joint details." in *Structures*. Elsevier, 2020.

[26] M.N. Hadi, H. Karim, and M.N. Sheikh, "Experimental investigations on circular concrete columns reinforced with GFRP bars and helices under different loading conditions." *Journal of Composites for Construction*, 20(4): p. 04016009, 2016.

[27] B. Benmokrane, O. Chaallal, and R. Masmoudi, "Glass fibre reinforced plastic (GFRP) rebars for concrete structures." *Construction and Building Materials*, 9(6): p. 353-364, 1995.

[28] A. Nour, et al., "Finite element modeling of concrete structures reinforced with internal and external fibre-reinforced polymers." *Canadian Journal of Civil Engineering*, 34(3): p. 340-354, 2007.

[29] T. Nguyen, T. Chan, and J. Mottram, "Influence of boundary conditions and geometric imperfections on lateral–torsional buckling resistance of a pultruded FRP I-beam by FEA." *Composite Structures*, 100: p. 233-242, 2013.

[30] J. Yang, T. Guo, and S. Chai. "Experimental and numerical investigation on seismic behaviours of beam-column joints of precast prestressed concrete frame under given corrosion levels." in *Structures*. Elsevier, 2020.

[31] A.M. Amiri, et al., "The effect of fly ash on flexural capacity concrete beams." *Advances in Science and Technology Research Journal*, 10(30), 2016.

[32] M. Najafgholipour, et al., "Finite element analysis of reinforced concrete beam-column connections with governing joint shear failure mode." *Latin American Journal of Solids and Structures*, 14(7): p. 1200-1225, 2017.

[33] M. Elflah, Theofanous, M., Dirar, S, Yuan, H., "Behaviour of stainless steel beam-to-column joints—Part 1: Experimental investigation." *Journal of Constructional Steel Research*, 152: p. 183-193, 2019.

[34] A. Niroomandi, M. Najafgholipour, and H.R. Ronagh, "Numerical investigation of the affecting parameters on the shear failure of Nonductile RC exterior joints." *Engineering Failure Analysis*, 46: p. 62-75, 2014.

[35] I.C. Muresan, and R. Balc. "Finite element analysis of an extended end-plate connection using the T-stub approach." in *AIP Conference Proceedings*. AIP Publishing, 2015.

[36. D.S. Simulia, Abaqus 6.12 documentation. Providence, Rhode Island, US, 2012. 261.

[37] M.Z. Afifi, Mohamed, H.M., Benmokrane, B., "Theoretical stress–strain model for circular concrete columns confined by GFRP spirals and hoops." *Engineering Structures*, 102: p. 202-213, 2015.

[38] A. Raza, Shah, SAR., Khan, AR., Aslam, MA., Khan, TA., Arshad, K., Hussan, S., Sultan, A., Shahzadi, G., Waseem, M., "Sustainable FRP-Confined Symmetric Concrete Structures: An Application Experimental and Numerical Validation Process for Reference Data." *Applied Sciences*, 10(1): p. 333, 2020.

[39] J. Wang, Chen, Y., ABAQUS application in civil engineering. 2006, Zhejiang University Press, China.

[40] Z. Huang, Liew, JYR., "Nonlinear finite element modelling and parametric study of curved steel-concrete-steel double skin composite panels infilled with ultra-lightweight cement composite." *Construction and Building Materials*, 95: p. 922-38, 2015.

[41] A. Raza, and Khan, QUZ, A. Ahmad, "Numerical Investigation of Load-Carrying Capacity of GFRP-Reinforced Rectangular Concrete Members Using CDP Model in ABAQUS." *Advances in Civil Engineering*, 2019, 2019.

[42] A.S. Genikomsou, and M.A. Polak, "Finite element analysis of punching shear of concrete slabs using damaged plasticity model in ABAQUS." *Engineering Structures*, 98: p. 38-48, 2015.

[43] J.Y. Wu, J. Li, and R. Faria, "An energy release rate-based plastic-damage model for concrete." *International journal of Solids and Structures*, 43(3-4): p. 583-612, 2006.

[44] G.Z. Voyiadjis, and Z.N. Taqieddin, "Elastic plastic and damage model for concrete materials: Part I-theoretical formulation." *The International Journal of Structural Changes in Solids*, 1(1): p. 31-59, 2009.

[45] R. Malm, "Predicting shear type crack initiation and growth in concrete with non-linear finite element method." KTH, 2009.

[46] D.S. Systèmes, Abaqus 6.10: Analysis user's manual. Providence, RI: Dassault Systèmes Simulia Corp, 2010.

[47] A. Raza, et al., "Structural performance of FRP-RC compression members wrapped with FRP composites." *Structures*, 27: p. 1693-1709, 2020.

[48] A. Raza, and Khan, QUZ, A. Ahmad, "Reliability analysis of proposed capacity equation for predicting the behavior of steel-tube concrete columns confined with CFRP sheets." *Computers and Concrete*, 25(5): p. 383-400, 2020.

[49] A. Raza, Shah, SAR., Alhazmi, H., Abrar, M., Razzaq, S. Strength Profile Pattern of FRP-Reinforced Concrete Structures: A Performance Analysis through Finite Element Analysis and Empirical Modeling Technique. *Polymers*, 13(8): 1265, 2021.

[50] A. Raza, et al., "Concentrically loaded recycled aggregate geopolymer concrete columns reinforced with GFRP bars and spirals." *Composite Structures*, 268: p. 113968, 2021.

[51] A. Raza, and U. Rafique, "Efficiency of GFRP bars and hoops in recycled aggregate concrete columns: Experimental and numerical study." *Composite Structures*. 255: p. 112986, 2020.

[52] A. Raza, et al., "Finite element modelling and theoretical predictions of FRP-reinforced concrete columns confined with various FRP-tubes." *Structures*,. 26: p. 626-638, 2020.

[53] L. Ali, et al., "Numerical Simulations of GFRP-Reinforced Columns Having Polypropylene and Polyvinyl Alcohol Fibers." *Complexity*, 2020, 2020.